ADVANCING EARTH AND SPACE SCIENCES

Geophysical Research Letters

RESEARCH LETTER
10.1029/2026GL122183

Resolving the Internal Magnetic Domain Structure of Cloudy Zone Tetrataenite

Elias N. Mansbach[1], **Richard J. Harrison**[1], **Tim A. Butcher**[2], **Simone Finizio**[3], **Sergio Valencia**[4], and **Thomas Ginnis**[1]

[1]Department of Earth Sciences, University of Cambridge, Cambridge, UK, [2]Max Born Institute for Nonlinear Optics and Short Pulse Spectroscopy, Berlin, Germany, [3]Swiss Light Source, Paul Scherrer Institut, Villigen, Switzerland, [4]Helmholtz-Zentrum Berlin für Materialien und Energie, Berlin, Germany

Key Points:

- We image the magnetic domain structures of cloudy zone tetrataenite at 4.4 nm resolution using soft X-ray dichroic ptychography
- The cloudy zone is comprised mostly of interacting, two-domain and higher-domain islands with single-domain structures in the minority
- The sub-10 nm resolution of X-ray dichroic ptychography opens numerous avenues of research into magnetic domain state behavior

Supporting Information:

Supporting Information may be found in the online version of this article.

Correspondence to:

E. N. Mansbach,
em2041@cam.ac.uk

Citation:

Mansbach, E. N., Harrison, R. J., Butcher, T. A., Finizio, S., Valencia, S., & Ginnis, T. (2026). Resolving the internal magnetic domain structure of cloudy zone tetrataenite. *Geophysical Research Letters*, *53*, e2026GL122183. https://doi.org/10.1029/2026GL122183

Received 30 JAN 2026
Accepted 19 APR 2026

Author Contributions:

Conceptualization: Elias N. Mansbach, Richard J. Harrison
Data curation: Elias N. Mansbach, Tim A. Butcher, Simone Finizio
Formal analysis: Elias N. Mansbach, Tim A. Butcher, Simone Finizio
Funding acquisition: Elias N. Mansbach
Investigation: Elias N. Mansbach, Richard J. Harrison, Tim A. Butcher, Simone Finizio, Sergio Valencia, Thomas Ginnis
Methodology: Elias N. Mansbach, Richard J. Harrison
Visualization: Elias N. Mansbach, Tim A. Butcher, Simone Finizio, Thomas Ginnis

Abstract

Recent advances in magnetic imaging can directly capture the internal magnetization of natural and synthetic materials at resolutions <10 nm. This capability opens new possibilities to determine the magnetic domain state of ferromagnetic minerals that are fundamental for recording and retaining paleomagnetic records. Here, we present the highest resolution magnetic contrast images to date of tetrataenite islands in the cloudy zone of the Esquel pallasite meteorite obtained using circular dichroic soft X-ray ptychography. These images, which have 4.4 nm spatial resolution, provide new insights into the magnetic structure of the cloudy zone, namely the prevalence of multidomain states, magnetostatic interactions, and islands with multiple "easy" magnetic axes. Our results demonstrate that the non-interacting, single-domain models used to derive cloudy-zone paleointensities in previous studies require re-evaluation. We additionally highlight the potential of high-resolution ptychography to enhance our understanding of paleomagnetic remanence carriers in future work.

Plain Language Summary

Magnetic imaging provides a method of seeing the internal magnetic structures of both natural and synthetic materials. New advances now allow us to take these images with a resolution below 10 nm. We apply one of these techniques, called X-ray ptychography, to image the magnetic structure of 150 nm "islands" of the mineral tetrataenite in an iron-bearing meteorite at 4.4 nm resolution. To determine the presence of an ancient magnetic field and its strength, previous studies of this mineral assumed that the islands occupied a uniform magnetization state and were non-interacting. However, these assumptions could not be tested as the previous studies used a magnetic imaging method that could not resolve the internal domain structure of the islands. Our magnetic imaging achieves this, and we find that most of the islands are not uniformly magnetized and interact with each other. Thus, existing ancient field intensity estimates should be reconsidered, and further work is needed to create models that accurately express how tetrataenite records magnetic fields. Additionally, we discuss the ways the geoscience community, particularly rock magnetists, could use ptychography to enhance our understanding of how minerals acquire and express their magnetic records.

1. Introduction

Since the creation of the Bitter method in 1932 (Bitter, 1932), numerous magnetic imaging techniques such as Magneto-optic Kerr effect (MOKE) and magnetic force microscopy (MFM) have been developed to determine the domain structures of natural minerals and industrial materials at increasingly higher spatial resolutions. Today, these advancements allow the magnetic imaging of materials down to <1 nm in the case of electron holography (McCartney & Smith, 2007) with MFM and MOKE achieving resolutions of ∼10 and ∼200 nm, respectively (Allwood et al., 2003; Kazakova et al., 2019). One downside to the above methods is that they do not image magnetization (M) directly. Instead, they either rely on detecting the magnetic induction (B) and using inversion techniques to recover M (e.g., electron holography) or detecting regions of rapidly changing B just above the sample surface to locate magnetic domain walls (e.g., MFM, MOKE, Bitter). However, measuring B rather than M is not ideal: inversions suffer from inherent non-uniqueness (Weiss et al., 2007) and can be more difficult to interpret, especially in the case of multiple, closely-packed sources (Bryson, Church, et al., 2014).

X-ray based techniques, on the other hand, can image magnetization directly but until recently have been unable to rival the spatial resolution achievable using, for example, electron holography. X-ray photoemission electron microscopy (XPEEM) typically provides surface-sensitive magnetization data down to 40 nm resolution (Bryson,

Writing – original draft: Elias N. Mansbach
Writing – review & editing: Elias N. Mansbach, Richard J. Harrison, Tim A. Butcher, Simone Finizio, Sergio Valencia, Thomas Ginnis

Herrero-Albillos, et al., 2014), though new generation PEEM systems can reach 5–10 nm depending on the sample (Niu et al., 2023). Similarly, X-ray Fourier transform holography typically provides 40 nm resolution (Blukis et al., 2020; Bryson, Herrero-Albillos, et al., 2014), but combining holography with phase retrieval techniques can achieve resolutions ∼5 nm (Battistelli et al., 2024). Notably, in the past decade soft X-ray dichroic ptychography has gained traction as a reliable method for determining the two-dimensional internal magnetization structures of natural minerals (Zhu et al., 2016) and synthetic materials (e.g., Butcher et al., 2024) at sub-10 nm resolutions and wide field of views. Combining ptychography with tomography (ptychotomography) now enables the three-dimensional magnetization vector field of magnetic materials to be constructed as well (resolution ∼20 nm) (Donnelly et al., 2017, 2018; Harrison et al., 2025).

The ability to image magnetization directly down to <10 nm resolution creates the opportunity to study the nanoscale domain structures of common ferromagnetic minerals that are fundamental to paleomagnetic investigations. This promises not only a greater understanding of mineral domain structures, but also insights into how paleofield records are initially captured by remanence carriers and how to accurately interpret these records. Here, we show the unique perspective these advances in magnetic imaging bring by utilizing soft X-ray dichroic ptychography to image the internal domains of nanoscale grains of tetrataenite (γ''-FeNi) in the "cloudy zone" (CZ) metallic microstructure, which comprises a densely packed intergrowth of tetrataenite "islands" embedded in an Fe-rich matrix. Tetrataenite is present in a wide variety of meteorite types including chondrites (e.g., Bryson et al., 2019), primitive achondrites (Mansbach et al., 2023), and iron meteorites (e.g., Goldstein et al., 2009), and has emerged as a popular ferromagnetic mineral for retrieving paleomagnetic information. This is primarily because of tetrataenite's high coercivity (>1 T for single-domain grains, Mansbach et al., 2022), which is due to the mineral's large magnetocrystalline anisotropy that effectively pins an island's magnetization along its crystallographic *c*-axis (Figure S1 in Supporting Information S1) (Bryson, Church, et al., 2014).

While the CZ has been used to determine the paleomagnetic history or magnetization of main group pallasites (Bryson et al., 2015; Nichols et al., 2016, 2021), mesosiderites (Nichols et al., 2020), an H chondrite (Bryson et al., 2019), and IIE (Maurel et al., 2020, 2021), IVA (Bryson et al., 2017), and IAB iron meteorites (Bryson, Herrero-Albillos, et al., 2014; Nichols et al., 2018), much remains unknown regarding how the tetrataenite in this system records its magnetization in the presence of a field, how that record is expressed, and how to calculate accurate paleointensities. For example, previous paleointensities have been primarily determined via a Maxwell-Boltzmann framework assuming non-interacting, single-domain islands that have their magnetization reset during ordering (Bryson et al., 2019). However, recent micromagnetic modeling indicates that many of the islands studied in existing experiments are more likely multidomain (Mansbach et al., 2022) and their magnetizations may be influenced by a precursor ferromagnetic phase rather than completely reset (Devienne et al., 2024).

The above uncertainties in part stem from the studies above utilizing XPEEM and therefore were unable to resolve the magnetization of individual islands (typically 10–100s nm). Below, we present the results of magnetic contrast images of CZ tetrataenite in the Esquel pallasite at a spatial resolution of 4.4 nm, an order of magnitude improvement compared to XPEEM. These images fully resolve the internal domain structure of the islands, providing new insights into the magnetization of tetrataenite and implications for previous CZ-based paleomagnetic studies. In addition, we discuss other avenues of research that could be conducted using X-ray ptychography that would benefit the geoscience community.

2. Materials and Methods

We used soft X-ray ptychography to obtain topographic and magnetic contrast images from the CZ in a 10 μm × 4 μm × 50–100 nm focused ion beam (FIB) section of the Esquel pallasite (Figures S2 and S3 in Supporting Information S1). Ptychographic reconstructions provided the complex transmission function of the sample (i.e., its amplitude and phase). The incoming photon energy was set to 702.75 eV (1.45 eV below the maximum observed Fe L_3-edge absorption, Figure S4 in Supporting Information S1). This configuration reduces the strong absorption expected at resonance for thick samples while still permitting its magnetic characterization by extracting X-ray magnetic circular dichroism (XMCD) values from the phase signal (Neethirajan et al., 2024).

Topographic images were computed by summing phase images taken at opposite helicities of the incident circularly polarized photon beam. Magnetic contrast images, representing the phase XMCD, were computed as the image difference. The resulting ptychographic XMCD images can resolve the internal domain structure of individual islands with a spatial resolution of 4.4 nm (Figure S5 in Supporting Information S1). Further details of

10.1029/2026GL122183

X-ray ptychography, the experimental setup, and the data processing to create the images can be found in Text S3 in Supporting Information S1 (Baruffaldi et al., 2025; Butcher et al., 2024, 2025a, 2025b, 2025c; Finizio et al., 2026). The FIB section thickness was chosen to be thinner than the average island diameter near the tetrataenite rim (~150 nm, Bryson et al., 2015), minimizing the chance of signal overlap from multiple islands as ptychography recovers information integrated through the sample in transmission. This meteorite was chosen due the large sizes of the islands relative to the expected spatial resolution of ptychography and since the paleomagnetic record of this meteorite has already been studied by Bryson et al. (2015), who conducted their investigation on the same sample used here (London Natural History Museum BM.1964,65). That investigation found a systematic bias in the magnetization of the islands, and calculated a paleointensity of 84 ± 14 μT, which was later revised to 64 ± 1.5 μT in Nichols et al. (2021).

3. Results

Figure 1 and Figure S6 in Supporting Information S1 show reconstructed topographic and phase-contrast XMCD images of the Esquel CZ at three adjacent regions of interest (ROIs), denoted ROI1, ROI2, and ROI3. In the following we discuss the results for ROI2, with comparable analyses for ROI1 and ROI3 and further information on the tetrataenite rim and matrix phases provided in Text S6–S8 in Supporting Information S1.

3.1. Domain States in the Cloudy Zone

Bright tetrataenite islands within the CZ are distinguished from the darker Fe-rich matrix in the topographic images (Figure 1a, Figure S7 in Supporting Information S1). The islands observed span from 50 to 230 nm in diameter and possess a range of nearly equant shapes to highly elongated structures with a width-to-length ratio of 0.25 (Figure 2b). The phase-contrast XMCD image (Figure 1b) reveals a mixture of single-domain and multidomain structures. Single-domain islands are identifiable due to their uniform phase XMCD, which manifests as narrow spikes in their corresponding pixel phase histograms (Figure 1e). Two-domain islands present a clear domain wall that splits the island into two separate uniformly magnetized regions, and their pixel phase histograms show two spikes of equal and opposite phase XMCDs centered around zero (Figure 1d, Figures S8 and S9 in Supporting Information S1). Lastly, we define higher-order domain structures as islands that are neither single- nor two-domain. These islands often contain multiple domain walls and complex, asymmetric pixel histograms (Figure 1c). Within ROI2, 32%, 46%, and 22% of the islands are classified as single-domain, two-domain, and higher-order domain, respectively, with similar values in the other ROIs (see Text S7 in Supporting Information S1).

In addition to various domain structures, we observe numerous examples of the presence of multiple c-axes within single islands in the XMCD images (Figures 1f and 1g). These islands are distinct from the two-domain islands above in that their peak phase XMCD values are not of equal magnitude and opposite polarity, and do not possess a clear domain wall, suggesting a relatively smooth transition in magnetization from one *c*-axis direction to another. We observe islands with multiple spikes of the same polarity (Figure 1g) or multiple sets centered around zero phase (Figure 1f). We classify these latter islands as higher-order domains as they tend to be larger and possess clear domain walls. The former islands (e.g., Figure 1g) are classified as single-domain as these islands are often smaller and there is no clear 180° domain wall present.

The average size of the islands decreases as the distance from the tetrataenite rim increases (Figure 2a, Figures S11 and S12 in Supporting Information S1). This change in size is matched by a consistent trend in the distribution of domain structures. Moving away from the interface in 1 μm steps, the proportion of single-domain islands increases from 21% to 35% while the proportion of higher-order domain islands decreases from 41% to 8% (Figure 2c). Despite the changes in domain structure distribution, single-domain islands never constitute the majority in any region. According to previous micromagnetic modeling of individual tetrataenite islands, the transition from single-domain to two-domain occurs at 80–135 nm depending on the axial ratio (Mansbach et al., 2022). However, 38 of the 114 single-domain islands in ROI2 plot outside of this region and in the two-domain stability region. We also find two-domain and higher-order domain islands within the predicted single-domain stability region (74% and 54% of identified two-domain and higher-order domain islands, respectively).

3.2. Distribution of c-Axes and Polarities

The high spatial resolution of our ptychographic images can determine the distribution of crystallographic *c*-axes in the CZ. This is seen in Figure 3a, which shows the histogram of phase XMCD for all islands in ROI2. Rather

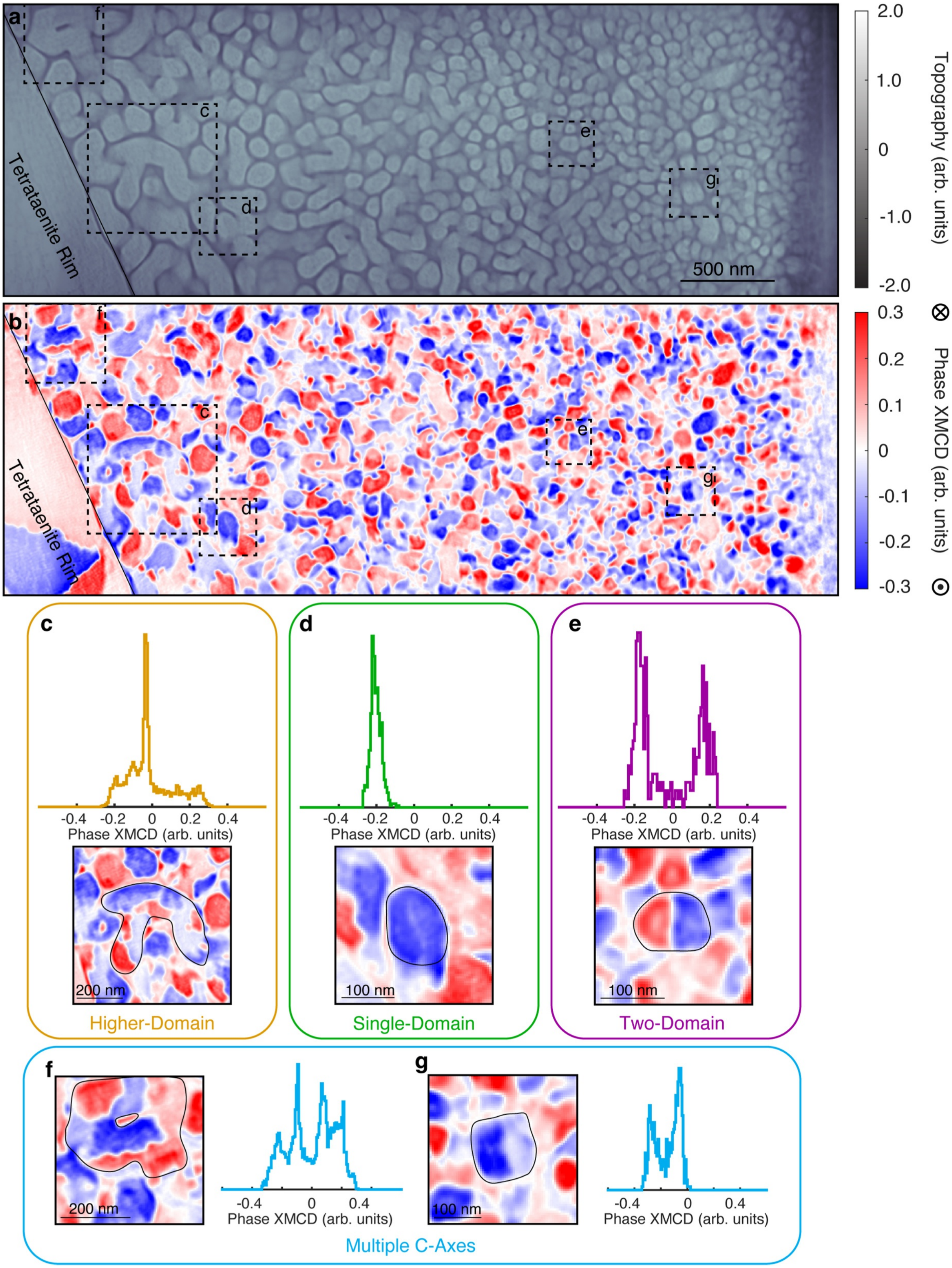

Figure 1. Summary of Tetrataenite Domain States. (a) Topographic image of ROI2. The tetrataenite island boundaries within the CZ are well-defined and can be identified. (b) X-ray magnetic circular dichroism (XMCD) image of the same field of view in (a). The phase XMCD value provides a measure of the component of magnetization of the islands along the X-ray beam (positive [negative] represents into [out of] plane). XMCD histograms and zoomed-in XMCD images of a higher-order domain (c), single-domain (d), and a two-domain (e) island. (f, g) Two examples of islands containing multiple c-axes.

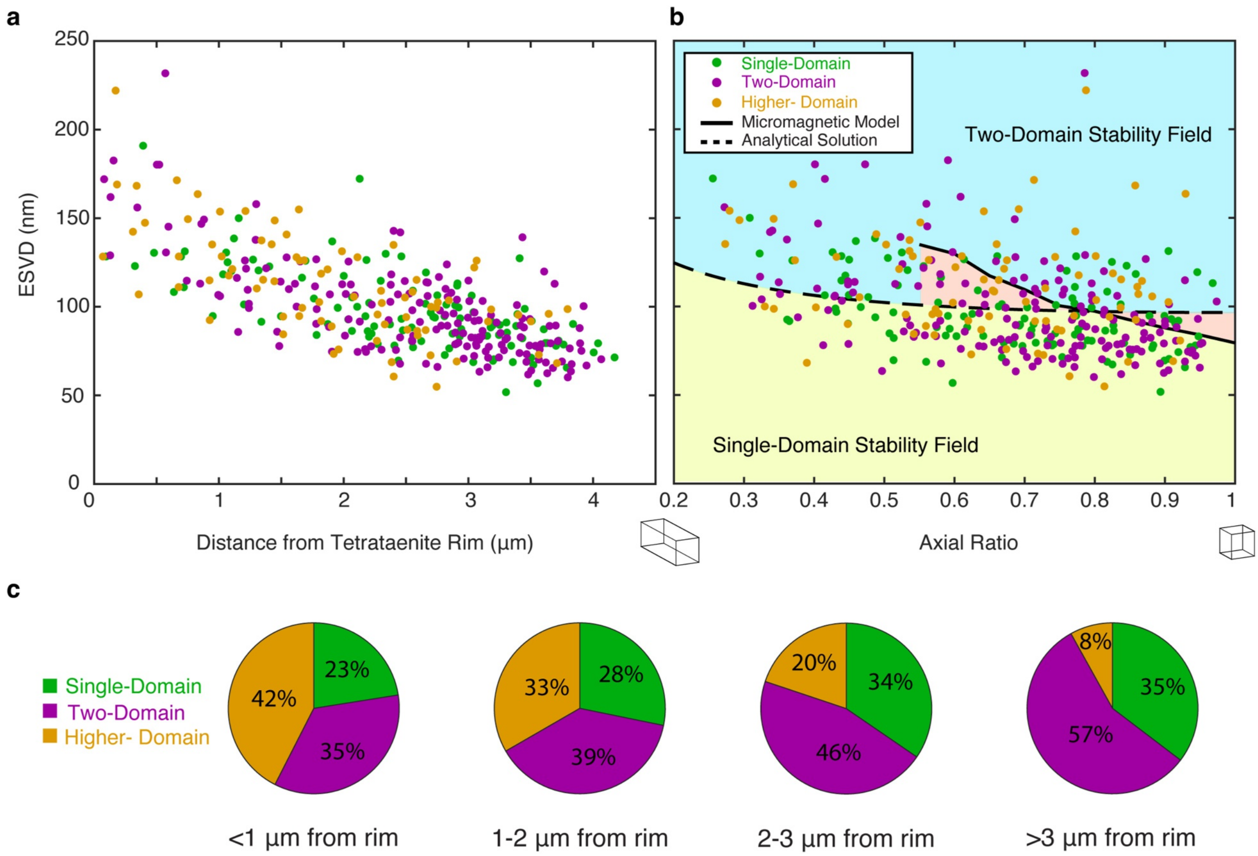

Figure 2. Size and Elongation of CZ Tetrataenite Islands. (a) Plot of island size as equivalent spherical volume diameter (ESVD) versus distance from the tetrataenite rim for ROI2. ESVD for each island calculated assuming the volume is the area observed in the topography image multiplied by the 75 nm estimated thickness of the focused ion beam section. Given the 25 nm uncertainty on the thickness, all ESVDs have an uncertainty of 9%. A decreasing trend in the island size with increasing distance from the rim is observed. (b) Plot of axial ratio (elongation) versus ESVD for islands in ROI2. While the majority of single-domain islands fall within the single-domain stability field (yellow shade), some are in the two-domain stability field (blude shade), providing evidence for magnetostatic interactions and the denucleation of domain walls (Devienne et al., 2024; Einsle et al., 2018; Mansbach et al., 2022). The micromagnetic model and analytical solution curves are taken from Mansbach et al. (2022). The red-shaded region shows the area where the micromagnetic model and analytical solution do not agree. (c) Pie charts of proportions of each domain state (single-domain, two-domain, and higher-order domain) in 1 µm increments from the tetrataenite rim.

than a single, broad peak as observed in pixel intensity histograms derived from XPEEM images of the CZ (Bryson et al., 2015), we observe multiple peaks indicative of individual *c*-axes. We determine the contribution from each *c*-axis through spectral decomposition of the histogram as a linear combination of six Gaussian distributions representing positive and negative polarities along each of the three possible *c*-axes (Figure 3b; see Text S8 in Supporting Information S1 for details). The pair of Gaussians with the lowest absolute mean phase XMCD magnitude are referred to as Axis 1, the middle as Axis 2, and the highest magnitude as Axis 3. Summing the areas under the Gaussians for positive and negative polarities for each *c*-axis, we observe a bias in all three ROIs toward Axis 2 since that axis has a total area above the 0.33 threshold expected for an equal distribution across all axes (Figure 3c). Within each pair of positive and negative axes, no consistent trend is observed in the ratio of areas for positive to negative polarities (Figure 3d). However, the recovered ratios span from 0.23 to 2.99, indicating significant asymmetries.

4. Discussion and Implications

4.1. Tetrataenite Domain States

The Esquel CZ is composed primarily of two-domain and higher-domain islands within 4 µm of the tetrataenite rim. The proportion of single-domain islands increases upon moving away from the rim though it is never the dominant domain state. Comparison of our results to previous micromagnetic modeling provides key insights into the nature of the CZ and tetrataenite island magnetic stability. First, numerous two-domain and higher-domain

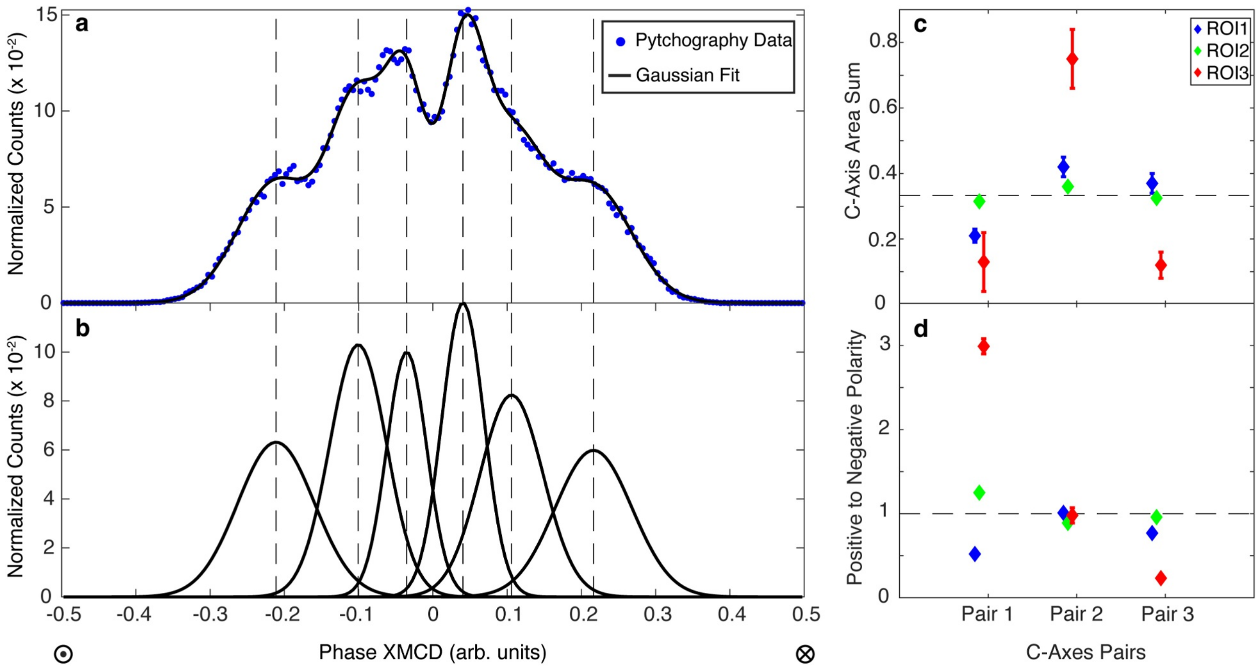

Figure 3. Gaussian Decomposition of phase X-ray magnetic circular dichroism (XMCD) values in ROI2. (a) Distribution of phase XMCD values from all islands within ROI2 (blue dots). The solid black line shows the best-fit of the linear superposition of six Gaussians. (b) The six Gaussians added together to create the best-fit to the data in (a). Each Gaussian distribution represents the contribution from one of six easy magnetization directions that tetrataenite may occupy. The vertical dashed black lines represent the centers of each gaussian distribution. (c) The summation of areas under each Gaussian curve for various *c*-axis pairs across the three regions of interest (ROIs). An equal distribution of *c*-axes would result in a value of 0.33 for each pair. (d) Ratios of the areas between polarities for each *c*-axis pair. An equal distribution of polarities would result in a value of 1 for each pair. Uncertainties shown are 95% confidence intervals. If no error bar is present, the uncertainty is smaller than the symbol.

islands fall into the single-domain stability region derived from modeling (Figure 2b) (Mansbach et al., 2022). This discrepancy may be explained by four mechanisms: (a) previous modeling of the single to two-domain threshold is incorrect; (b) our determination of the diameter was sourced from the topographic image, which is two-dimensional (i.e., the island is thicker); (c) the islands were initially larger but then thinned down to a smaller size during the making of the FIB slice while still retaining a non-single-domain structure; or (d) the islands occupy a metastable two-domain state.

We suggest that the latter two explanations are more likely since, for the third mechanism, micromagnetic modeling of an initially two-domain, 150 nm diameter tetrataenite island shows that the domain structure is retained during progressive thinning of the island, either from one direction or from two directions, to at least 50% and 20% of the initial volume, respectively, depending on the direction of thinning relative to the *c*-axis (Figures S15 and S16, Text S9 in Supporting Information S1). This is also the case for islands modeled containing multiple *c*-axes and three domains (Figure S17 in Supporting Information S1). This suggests that tetrataenite can retain its domain state at smaller sizes after FIB sectioning or polishing prior to synchrotron measurement, a concern raised during the initial formulation of the CZ as a paleomagnetic tool (Bryson, Herrero-Albillos, et al., 2014). However, the remanence may be affected by domain wall movement depending on the direction of thinning relative to the *c*-axis (Figures S15–S17 in Supporting Information S1). With regard to the fourth mechanism, previous micromagnetic modeling of the transition from single-vortex taenite to tetrataenite at island sizes below the tetrataenite single- to two-domain transition indicates that, depending on the ordering direction, the final state could be a two-domain or single-domain island (Devienne et al., 2024; Einsle et al., 2018). The two-domain state would be considered metastable as it is not the global minimum energy state for that size, but the energy barrier to relaxation into a single-domain state corresponds to a time period longer than the lifetime of the solar system and therefore could be observed today (Mansbach et al., 2022).

Next, we observe numerous instances of single-domain islands that fall into the two-domain stability region in Figure 2b. This finding provides the first observational evidence for predictions derived from micromagnetic modeling that if a two-domain island is transformed into a single-domain state via domain wall denucleation, the island will remain single-domain and not renucleate a domain wall even if the external field is removed. In the context of the CZ, the most likely method of achieving domain wall denucleation is through stray fields produced by one island on its neighbor since the required field is 100s of mT, much larger than any known planetesimal field (Einsle et al., 2018; Mansbach et al., 2022). The identification of large single-domain islands is therefore strong evidence that magnetostatic interactions influence the domain structure and magnetization of CZ islands. We acknowledge that an alternative method of producing a large single-domain island is through taenite to tetrataenite ordering along the *c*-axis (Devienne et al., 2024), though further evidence for magnetostatic interactions comes from hysteresis measurements of the CZ using X-ray holography (Blukis et al., 2020).

4.2. Impact of Ptychographic Imaging on Previous Cloudy Zone Investigations

Previous CZ XPEEM studies have determined paleointensities by comparing XMCD intensities to the expected results from a Maxwell-Boltzmann distribution of magnetization directions along each of the three potential crystallographic *c*-axes (see Bryson et al., 2019 for full explanation). While there are numerous shortcomings of this framework (see Text S10 in Supporting Information S1), here we focus on two assumptions addressed by our high-resolution magnetic images. First, the Maxwell-Boltzmann approach assumes that all islands occupy a single domain aligned in one of six directions. Allowing for multidomain islands or islands with multiple *c*-axes as observed in Figure 1 greatly expands the possible magnetic states that each island can occupy as the magnetizations of the islands will vary depending on the location of the domain wall or *c*-axis interface. We note as well that the identification of multiple *c*-axes in individual islands supports the hypothesis that tetrataenite forms from a nucleation and growth process starting either at the edge of, or within, the precursor taenite (Devienne et al., 2024). Multiple *c*-axes may be the result of various nucleation points that leads to ordering along more than one Fe-Ni plane simultaneously in different regions of one island (Figure S19 in Supporting Information S1). This also highlights the potential importance of taenite remanence on the product tetrataenite magnetization (Devienne et al., 2024) if the taenite magnetization influences the ordering direction of the tetrataenite (see next subsection).

Second, the Maxwell-Boltzmann framework assumes the islands are not interacting such that the magnetization of one island has no effect on its neighbor. As described in the previous subsection, our results provide strong evidence that magnetostatic interactions are present and affect island magnetization. That said, the degree to which magnetostatic interactions influence the ability of CZ tetrataenite to record external fields remains the subject of further study. The interaction fields between islands are up to five orders of magnitude stronger than any planetary field (Mansbach et al., 2022), which would seemingly mask the imprint from an external field. However, Maurel et al. (2020) point out two reasons why XPEEM studies indicate that interactions should not prevent the recording of a paleofield. First, average CZ remanent magnetization directions across multiple interfaces in the same meteorite sample show unidirectionality, which would not likely be the case if interactions were the driving factor in CZ remanence. Second, previous XPEEM experiments have detected both CZs with distinguishable biases from zero (e.g., Bryson et al., 2015) and CZs with indistinguishable biases (e.g., Nichols et al., 2016), though we note that null-field detections have only occurred during data collection along one X-ray beam direction, which is important as the direction of the beam relative to the surface influences the observed pixel intensity distribution as seen in Maurel et al. (2020). If magnetostatic interactions were the source of CZ remanence, one would expect XMCD average intensities to always deviate from zero. It is for these reasons that despite the findings here regarding the prevalence of multidomain tetrataenite and interactions in the CZ, we conclude that the CZ can still indicate the presence or absence of a field, but quantitative paleointensity estimates are not robust under the previous assumptions. A new model of the magnetization mechanism of the CZ is now needed that takes full account of the domain states and interactions identified here.

4.3. Soft X-Ray Ptychography as a CZ Paleomagnetic Technique

The high spatial resolution of soft X-ray ptychography enables direct determination of the magnetization of individual tetrataenite islands. Unlike XPEEM XMCD imaging, which expresses pixel intensities averaged over many islands (Figure S20 in Supporting Information S1), ptychography allows the net magnetic moment of the cloudy zone to be determined without domain state assumptions. This makes it a promising technique for paleomagnetic studies of the CZ in the future.

In our ptychographic XMCD data, we observe a consistent bias toward one *c*-axis direction but no systematic polarity preference along that axis or the other two axes across the three ROIs. If a paleofield was present, one may expect the islands along each *c*-axis to prefer the polarity closest to the field direction in each ROI given their proximity. Thus, our results do not provide clear evidence for an external field in contrast with a previous XPEEM study of the same sample (Bryson et al., 2015). Three factors may explain this discrepancy. First, ROIs in prior CZ studies are typically defined as 500 nm–2 μm regions parallel to the rim to sample islands of uniform size (Bryson et al., 2015; Maurel et al., 2020). Here, we defined ROIs nearly perpendicular to the rim, as data merging along the rim was not feasible due to lack of significant overlap between ROIs, and dividing the ROIs into rim-parallel regions would yield too few islands per subset. Second, the total number of islands analyzed here (668, with some double-counted at ROI boundaries) is substantially lower than the thousands typically imaged in XPEEM studies (e.g., Maurel et al., 2020), limiting statistical power (see Text S14 in Supporting Information S1). Lastly, thinning of the island can cause shifts in the magnetization depending on the thinning direction relative to the island *c*-axis (see Text S9 in Supporting Information S1).

We note that the observed bias toward a consistent *c*-axis may be indicative of formation in an external field environment as density functional theory simulations of tetrataenite ordering show a preference for ordering along the direction of the precursor taenite magnetization (Woodgate et al., 2023). However, we caution that this result was for a uniformly magnetized grain at volumes far lower than the islands observed here, which we would expect to be larger and occupy a vortex state as taenite (Devienne et al., 2023). Additional ptychography images collected on CZs with and without reported field detections may establish the relationship between *c*-axis distribution and the presence or absence of an external field.

4.4. A New Way to Study Rock Magnetism

The ability of soft X-ray dichroic ptychography to resolve the internal domain structure of ferromagnetic minerals at sub-10 nm resolutions opens numerous future avenues of research within the paleomagnetism and rock magnetism communities that will greatly enhance our understanding of how minerals retain magnetic records. For example, current methods of determining the dominant domain state in bulk samples rely either on proxy techniques, such as first-order reversal curves (Muxworthy & Roberts, 2007) and other products of hysteresis loops (i.e., Day diagrams), or by comparing the sizes and shapes of known ferromagnetic particles to diagrams determined through analytical calculations (e.g., Butler & Banerjee, 1975) and micromagnetic modeling (e.g., Muxworthy & Williams, 2006). Soft X-ray ptychography allows the direct testing of these methods through the imaging of particles with various morphologies and diameters, thereby verifying or changing our understanding of how domains evolve with size.

An additional benefit of soft X-ray ptychography and other X-ray imaging techniques is that they can be conducted in the presence of an external field. Domain state imaging of grains in the presence of an increasing field will provide key information into vortex core and domain wall movement that can lead to new models to assess how bulk samples experience remagnetization or demagnetization, and test current models of domain wall movement as well (Berndt & Chang, 2018). This is particularly important for the CZ, as it is proposed that large single-domain grains form as the result of domain wall denucleation through magnetostatic interactions as discussed above. Future studies can also take advantage of the ability to conduct soft X-ray ptychography during sample heating. This will create new insights into how domains change in response to increasing temperature and how to interpret thermal demagnetizations of bulk rocks. In addition, it will provide an opportunity to test the veracity of energy barriers calculated using micromagnetic models that are typically used to determine the stability of paleomagnetic records (i.e., Nagy et al., 2017).

5. Conclusions

Recent advances in magnetic imaging now allow the determination of the internal magnetic domain structure of individual nanoparticles. Here, we utilize soft X-ray ptychography to image the domain structure of individual tetrataenite islands in the Esquel pallasite at sub-10 nm spatial resolution. We find that the CZ is dominated by two-domain and higher-domain tetrataenite, with further evidence for strong magnetostatic interactions between islands. In addition, we observe numerous instances of islands containing multiple *c*-axes. Our results indicate that previous assumptions taken to calculate paleointensities from the CZ are invalid and therefore new models to convert experimental observations into quantitative paleointensity estimates are urgently needed. Additionally, further experimental work is required to constrain how external fields influence multidomain tetrataenite. Our results also suggest that soft X-ray ptychography can be a novel method of conducting paleomagnetic studies of the CZ if a statistically meaningful number of islands are imaged, and Gaussian deconvolution of XMCD histograms could reveal preferred *c*-axes and polarities. Our results additionally exemplify the power and utility of high-resolution magnetic imaging in furthering our understanding of how paleomagnetic systems acquire and express their magnetizations. Future work may implement X-ray ptychography to directly study how domains change with grain morphology and size, and how ferromagnetic minerals respond to external fields and heating.

Conflict of Interest

The authors declare no conflicts of interest relevant to this study.

Availability Statement

The raw data used to create the phase sum and XMCD images, in addition to the raw phase images themselves, have been placed in one location accessible via the Harvard Dataverse at https://dataverse.harvard.edu/dataset.xhtml?persistentId=doi:10.7910/DVN/LQKVF8 (Mansbach et al., 2026).

Acknowledgments
ENM acknowledges the Herchel Smith Postdoctoral Fellowship program for funding for this work. RJH and TG acknowledge funding from the European Union's Horizon Europe research and innovation program under grant agreement No. 101131765 (EXCITE^2) and Grants G106564 and G122171. T.A.B. acknowledges funding from the European Regional Development Fund. The authors thank Iris Busiman and Rosa Danisi for assistance with electron microscopy imaging and the Natural History Museum London (curator Mark Boyd) for providing a sample for this study. Development of SOPHIE was financially supported by the Swiss Nanoscience Institute (SNI). We acknowledge the support of the Wolfson Electron Microscopy Suite and use of the FEI Helios for FIB-section making at the Department of Material Sciences and Metallurgy, University of Cambridge. We additionally thank Fengzai Tang and the Warwick Manufacturing Group at the University of Warwick for preparation of an earlier test sample that led to the optimized sample thickness used in this study. We acknowledge the MAX IV Laboratory (Lund, Sweden) for beamtime on the SoftiMAX beamline. Research conducted at MAX IV, a Swedish national user facility, is supported by the Swedish Research Council under contract 2018-07152, the Swedish Governmental Agency for Innovation Systems under contract 2018–04969, and Formas under contract 2019-02496. We thank I. Beinik, C. Bulbucan, and K. Thånell for support at the SoftiMAX beamline. We thank E. Fröjdh, F. Baruffaldi, M. Carulla, J. Zhang, and A. Bergamaschi for the development of the iLGAD EIGER detector. The iLGAD sensors were fabricated at Fondazione Bruno Kessler (Trento, Italy). Lastly, thank Clara Maurel and Claire Nichols for providing insightful and constructive reviews that increased the quality and clarity of the manuscript.

References

Allwood, D. A., Xiong, G., Cooke, M. D., & Cowburn, R. P. (2003). Magneto-optical Kerr effect analysis of magnetic nanostructures. *Journal of Physics D: Applied Physics*, *36*(18), 2175–2182. https://doi.org/10.1088/0022-3727/36/18/001
Baruffaldi, F., Bergamaschi, A., Boscardin, M., Brückner, M., Butcher, T. A., Carulla, M., et al. (2025). Single-photon counting pixel detector for soft X-rays. *Communications Physics*, *8*(1), 321. https://doi.org/10.1038/s42005-025-02240-9
Battistelli, R., Metternich, D., Schneider, M., Kern, L.-M., Litzius, K., Fuchs, J., et al. (2024). Coherent X-ray magnetic imaging with 5 nm resolution. *Optica*, *11*(2), 234–237.
Berndt, T. A., & Chang, L. (2018). Theory of stable multidomain thermoviscous remanence based on repeated domain wall jumps. *Journal of Geophysical Research: Solid Earth*, *123*(12). https://doi.org/10.1029/2018jb016816
Bitter, F. (1932). Experiments on the nature of ferromagnetism. *Physical Review*, *41*(4), 507–515. https://doi.org/10.1103/physrev.41.507
Blukis, R., Pfau, B., Günther, C. M., Hessing, P., Eisebitt, S., Einsle, J., & Harrison, R. J. (2020). Nanoscale imaging of high-field magnetic hysteresis in meteoritic metal using X-ray holography. *Geochemistry, Geophysics, Geosystems*, *21*(8), e2020GC009044. https://doi.org/10.1029/2020gc009044
Bryson, J. F. J., Church, N. S., Kasama, T., & Harrison, R. J. (2014). Nanomagnetic intergrowths in Fe–Ni meteoritic metal: The potential for time-resolved records of planetesimal dynamo fields. *Earth and Planetary Science Letters*, *388*, 237–248. https://doi.org/10.1016/j.epsl.2013.12.004
Bryson, J. F. J., Herrero-Albillos, J., Kronast, F., Ghidini, M., Redfern, S. A. T., van der Laan, G., & Harrison, R. J. (2014). Nanopaleomagnetism of meteoritic Fe–Ni studied using X-ray photoemission electron microscopy. *Earth and Planetary Science Letters*, *396*, 125–133. https://doi.org/10.1016/j.epsl.2014.04.016
Bryson, J. F. J., Nichols, C. I. O., Herrero-Albillos, J., Kronast, F., Kasama, T., Alimadadi, H., et al. (2015). Long-lived magnetism from solidification-driven convection on the pallasite parent body. *Nature*, *517*(7535), 472–475. https://doi.org/10.1038/nature14114
Bryson, J. F. J., Weiss, B. P., Getzin, B., Abrahams, J. N. H., Nimmo, F., & Scholl, A. (2019). Paleomagnetic evidence for a partially differentiated ordinary chondrite parent asteroid. *Journal of Geophysical Research*, *124*(7), 1880–1898. https://doi.org/10.1029/2019je005951
Bryson, J. F. J., Weiss, B. P., Harrison, R. J., Herrero-Albillos, J., & Kronast, F. (2017). Paleomagnetic evidence for dynamo activity driven by inward crystallisation of a metallic asteroid. *Earth and Planetary Science Letters*, *472*, 152–163. https://doi.org/10.1016/j.epsl.2017.05.026
Butcher, T. A., Finizio, S., Heller, L., Phillips, N. W., Sarafimov, B., Vaz, C. A. F., et al. (2025). Soft X-ray ptychography with SOPHIE: Guide and instrumentation. *Review of Scientific Instruments*, *96*(12), 123704. https://doi.org/10.1063/5.0303529
Butcher, T. A., Phillips, N. W., Chiu, C. C., Wei, C. C., Ho, S. Z., Chen, Y. C., et al. (2024). Ptychographic nanoscale imaging of the magnetoelectric coupling in freestanding $BiFeO_3$. *Advanced Materials*, *36*(23), e2311157. https://doi.org/10.1002/adma.202311157
Butcher, T. A., Phillips, N. W., Levitan, A. L., Weigand, M., Wintz, S., Raabe, J., & Finizio, S. (2025). Nanoscale domain-wall dynamics in micromagnetic structures with weak perpendicular anisotropy. *Physical Review B*, *111*(22), L220409. https://doi.org/10.1103/2y4r-my27
Butcher, T. A., Phillips, N. W., Wei, C.-C., Chang, S.-C., Beinik, I., Thånell, K., et al. (2025). Imaging ferroelectric domains with soft-X-ray ptychography at the oxygen K-edge. *Physical Review Applied*, *23*(1), L011002. https://doi.org/10.1103/physrevapplied.23.l011002
Butler, R. F., & Banerjee, S. K. (1975). Theoretical single-domain grain size range in magnetite and titanomagnetite. *Journal of Geophysical Research*, *80*(29), 4049–4058. https://doi.org/10.1029/jb080i029p04049
Devienne, J. A. P. M., Berndt, T. A., Williams, W., & Chen, S. (2024). From disorder to order: Inheritance of magnetic remanence in tetrataenite-bearing meteorites from multi-phase micromagnetic modeling. *Journal of Geophysical Research: Planets*, *129*(6), e2023JE008268. https://doi.org/10.1029/2023je008268
Devienne, J. A. P. M., Berndt, T. A., Williams, W., & Nagy, L. (2023). Magnetic recording stability of taenite-containing meteorites. *Geophysical Research Letters*, *50*(12), e2022GL102602. https://doi.org/10.1029/2022gl102602
Donnelly, C., Gliga, S., Scagnoli, V., Holler, M., Raabe, J., Heyderman, L. J., & Guizar-Sicairos, M. (2018). Tomographic reconstruction of a three-dimensional magnetization vector field. *New Journal of Physics*, *20*(8), 083009. https://doi.org/10.1088/1367-2630/aad35a
Donnelly, C., Guizar-Sicairos, M., Scagnoli, V., Gliga, S., Holler, M., Raabe, J., & Heyderman, L. J. (2017). Three-dimensional magnetization structures revealed with X-ray vector nanotomography. *Nature*, *547*(7663), 328–331. https://doi.org/10.1038/nature23006
Einsle, J. F., Eggeman, A. S., Martineau, B. H., Saghi, Z., Collins, S. M., Blukis, R., et al. (2018). Nanomagnetic properties of the meteorite cloudy zone. *Proceedings of the National Academy of Sciences*, *115*(49), E11436–E11445. https://doi.org/10.1073/pnas.1809378115
Finizio, S., Butcher, T. A., Cocconcelli, M., Müller, E., Riddiford, L. J., Brock, J. A., et al. (2026). In situ straining of epitaxial freestanding ferroic films by a microelectromechanical device. *Physical Review B*, *113*(13), 134408. https://doi.org/10.1103/pj3y-qfvb

Goldstein, J. I., Scott, E. R. D., & Chabot, N. L. (2009). Iron meteorites: Crystallization, thermal history, parent bodies, and origin. *Geochemistry*, *69*(4), 293–325. https://doi.org/10.1016/j.chemer.2009.01.002

Harrison, R. J., Neethirajan, J., Pei, Z., Xue, P., Marcano, L., Abrudan, R., et al. (2025). Magnetic vector tomography reveals giant magnetofossils are optimised for magnetointensity reception. *Communications Earth & Environment*, *6*(1), 810. https://doi.org/10.1038/s43247-025-02721-3

Kazakova, O., Puttock, R., Barton, C., Corte-León, H., Jaafar, M., Neu, V., & Asenjo, A. (2019). Frontiers of magnetic force microscopy. *Journal of Applied Physics*, *125*(6), 060901. https://doi.org/10.1063/1.5050712

Mansbach, E. N., Harrison, R. J., Butcher, T. A., Finizio, S., Valencia, S., & Ginnis, T. (2026). Data repository for resolving the internal magnetic domain structure of cloudy zone tetrataenite.

Mansbach, E. N., Shah, J., Williams, W., Maurel, C., Bryson, J. F. J., & Weiss, B. P. (2022). Size ranges of magnetic domain states in tetrataenite. *Geochemistry, Geophysics, Geosystems*, *23*(11), e2022GC010631. https://doi.org/10.1029/2022gc010631

Mansbach, E. N., Weiss, B. P., Schnepf, N. R., Lima, E. A., Borlina, C. S., Chatterjee, N., et al. (2023). Magnetism of the Acapulco primitive achondrite and implications for the evolution of partially differentiated bodies. *Journal of Geophysical Research: Planets*, *128*(12), e2023JE008076. https://doi.org/10.1029/2023je008076

Maurel, C., Bryson, J. F. J., Lyons, R. J., Ball, M. R., Chopdekar, R. V., Scholl, A., et al. (2020). Meteorite evidence for partial differentiation and protracted accretion of planetesimals. *Science Advances*, *6*(30), eaba1303. https://doi.org/10.1126/sciadv.aba1303

Maurel, C., Bryson, J. F. J., Shah, J., Chopdekar, R. V., Elkins, T., Tanton, L., et al. (2021). A long-lived planetesimal dynamo powered by core crystallization. *Geophysical Research Letters*, *48*(6), e2020GL091917. https://doi.org/10.1029/2020gl091917

McCartney, M. R., & Smith, D. J. (2007). Electron holography: Phase imaging with nanometer resolution. *Annual Review of Materials Research*, *37*(1), 729–767. https://doi.org/10.1146/annurev.matsci.37.052506.084219

Muxworthy, A. R., & Roberts, A. P. (2007). First-order reversal curve (FORC) diagrams. In D. Gubbins & E. Herrero-Bervera (Eds.), *Encyclopedia of geomagnetism and paleomagnetism* (pp. 266–272). Springer.

Muxworthy, A. R., & Williams, W. (2006). Critical single-domain/multidomain grain sizes in noninteracting and interacting elongated magnetite particles: Implications for magnetosomes. *Journal of Geophysical Research*, *111*(B12), B12S12. https://doi.org/10.1029/2006jb004588

Nagy, L., Williams, W., Muxworthy, A. R., Fabian, K., Almeida, T. P., Conbhuí, P. Ó., & Shcherbakov, V. P. (2017). Stability of equidimensional pseudo–single-domain magnetite over billion-year timescales. *Proceedings of the National Academy of Sciences*, *114*(39), 10356–10360. https://doi.org/10.1073/pnas.1708344114

Neethirajan, J., Daurer, B. J., Martínez, M. D. P., Hrabec, A., Turnbull, L., Yamamoto, R., et al. (2024). Soft X-ray phase nanomicroscopy of micrometer-thick magnets. *Physical Review X*, *14*(3), 031028. https://doi.org/10.1103/physrevx.14.031028

Nichols, C. I. O., Bryson, J. F. J., Blukis, R., Herrero-Albillos, J., Kronast, F., Rüffer, R., et al. (2020). Variations in the magnetic properties of meteoritic cloudy zone. *Geochemistry, Geophysics, Geosystems*, *21*(2), e2019GC008798. https://doi.org/10.1029/2019gc008798

Nichols, C. I. O., Bryson, J. F. J., Cottrell, R. D., Fu, R. R., Harrison, R. J., Herrero-Albillos, J., et al. (2021). A time-resolved paleomagnetic record of main group pallasites: Evidence for a large-cored, thin-mantled parent body. *Journal of Geophysical Research: Planets*, *126*(7), e2021JE006900. https://doi.org/10.1029/2021je006900

Nichols, C. I. O., Bryson, J. F. J., Herrero-Albillos, J., Kronast, F., Nimmo, F., & Harrison, R. J. (2016). Pallasite paleomagnetism: Quiescence of a core dynamo. *Earth and Planetary Science Letters*, *441*, 103–112. https://doi.org/10.1016/j.epsl.2016.02.037

Nichols, C. I. O., Krakow, R., Herrero-Albillos, J., Kronast, F., Northwood-Smith, G., & Harrison, R. J. (2018). Microstructural and paleomagnetic insight into the cooling history of the IAB parent body. *Geochimica et Cosmochimica Acta*, *229*, 1–19. https://doi.org/10.1016/j.gca.2018.03.009

Niu, Y., Vinogradov, N., Preobrajenski, A., Struzzi, C., Sarpi, B., Zhu, L., et al. (2023). MAXPEEM: A spectromicroscopy beamline at MAX IV laboratory. *Journal of Synchrotron Radiation*, *30*(2), 468–478.

Weiss, B. P., Lima, E. A., Fong, L. E., & Baudenbacher, F. J. (2007). Paleomagnetic analysis using SQUID microscopy. *Journal of Geophysical Research*, *112*(B9). https://doi.org/10.1029/2007jb004940

Woodgate, C. D., Patrick, C. E., Lewis, L. H., & Staunton, J. B. (2023). Revisiting Néel 60 years on: The magnetic anisotropy of $L1_0$ FeNi (tetrataenite). *Journal of Applied Physics*, *134*(16), 163905. https://doi.org/10.1063/5.0169752

Zhu, X., Hitchcock, A. P., Bazylinski, D. A., Denes, P., Joseph, J., Lins, U., et al. (2016). Measuring spectroscopy and magnetism of extracted and intracellular magnetosomes using soft X-ray ptychography. *Proceedings of the National Academy of Sciences*, *113*(51), E8219–E8227. https://doi.org/10.1073/pnas.1610260114

References From the Supporting Information

Berndt, T. A., Muxworthy, A. R., & Fabian, K. (2016). Does size matter? Statistical limits of paleomagnetic field reconstruction from small rock specimens: Does size matter? *Journal of Geophysical Research*, *121*(1), 15–26. https://doi.org/10.1002/2015jb012441

Blukis, R., Ruffer, R., Chumakov, A. I., & Harrison, R. J. (2017). A high spatial resolution synchrotron Mossbauer study of the Tazewell IIICD and Esquel pallasite meteorites. *Meteoritics & Planetary Science*, *52*(5), 925–936. https://doi.org/10.1111/maps.12841

Clarke, R. S., & Scott, E. R. D. (1980). Tetrataenite—Ordered FeNi, a new mineral in meteorites. *American Mineralogist*, *65*(7–8), 624–630.

Conbhuí, P. Ó., Williams, W., Fabian, K., Ridley, P., Nagy, L., & Muxworthy, A. R. (2018). MERRILL: Micromagnetic Earth related robust interpreted language laboratory. *Geochemistry, Geophysics, Geosystems*, *19*(4), 1080–1106. https://doi.org/10.1002/2017gc007279

Goldstein, J. I., & Michael, J. R. (2006). The formation of plessite in meteoritic metal. *Meteoritics & Planetary Science*, *41*(4), 553–570. https://doi.org/10.1111/j.1945-5100.2006.tb00482.x

Hubert, A., & Schäfer, R. (1998). *Magnetic domains: The analysis of magnetic microstructures*. Springer Berlin.

Maurel, C., Weiss, B. P., & Bryson, J. F. J. (2019). Meteorite cloudy zone formation as a quantitative indicator of paleomagnetic field intensities and cooling rates on planetesimals. *Earth and Planetary Science Letters*, *513*, 166–175. https://doi.org/10.1016/j.epsl.2019.02.027

Miao, J. (2025). Computational microscopy with coherent diffractive imaging and ptychography. *Nature*, *637*(8045), 281–295. https://doi.org/10.1038/s41586-024-08278-z

Néel, L., Pauleve, J., Pauthenet, R., Laugier, J., & Dautreppe, D. (1964). Magnetic properties of an iron—Nickel single crystal ordered by neutron bombardment. *Journal of Applied Physics*, *35*(3), 873–876. https://doi.org/10.1063/1.1713516

Odstrčil, M., Menzel, A., & Guizar-Sicairos, M. (2018). Iterative least-squares solver for generalized maximum-likelihood ptychography. *Optics Express*, *26*(3), 3108–3123. https://doi.org/10.1364/oe.26.003108

Pokhil, T. G., & Moskowitz, B. M. (1997). Magnetic domains and domain walls in pseudo-single-domain magnetite studied with magnetic force microscopy. *Journal of Geophysical Research*, *102*(B10), 22681–22694. https://doi.org/10.1029/97jb01856

Preibisch, S., Saalfeld, S., & Tomancak, P. (2009). Globally optimal stitching of tiled 3D microscopic image acquisitions. *Bioinformatics*, *25*(11), 1463–1465. https://doi.org/10.1093/bioinformatics/btp184

Thibault, P., Dierolf, M., Menzel, A., Bunk, O., David, C., & Pfeiffer, F. (2008). High-resolution scanning X-ray diffraction microscopy. *Science*, *321*(5887), 379–382. https://doi.org/10.1126/science.1158573

Thibault, P., & Menzel, A. (2013). Reconstructing state mixtures from diffraction measurements. *Nature*, *494*(7435), 68–71. https://doi.org/10.1038/nature11806

van Heel, M., & Schatz, M. (2005). Fourier shell correlation threshold criteria. *Journal of Structural Biology*, *151*(3), 250–262. https://doi.org/10.1016/j.jsb.2005.05.009

Wakonig, K., Stadler, H. C., Odstrcil, M., Tsai, E. H. R., Diaz, A., Holler, M., et al. (2020). Ptychoshelves, a versatile high-level framework for high-performance analysis of ptychographic data. *Journal of Applied Crystallography*, *53*(Pt 2), 574–586. https://doi.org/10.1107/s1600576720001776

Yang, C. W., Williams, D. B., & Goldstein, J. I. (1997). Low-temperature phase decomposition in metal from iron, stony-iron, and stony meteorites. *Geochimica et Cosmochimica Acta*, *61*(14), 2943–2956. https://doi.org/10.1016/s0016-7037(97)00132-4